Annual Report on Contract NAS8-35667

entitled:

COSMIC RAY ASTRONOMY AND

ENERGETIC PARTICLE INTERACTIONS

Reporting Period:

1/17/84 - 1/16/85

Cosmic Ray Laboratory

Chemistry Department

The University of Alabama in Huntsville

INTRODUCTION

Nuclear track emulsions, with their unparalleled spatial resolution for multiple charged tracks have a long and continuing history of application to the study of nucleus-nucleus interactions at high energy. Much of this work has been carried out on high-altitude balloons by exposing emulsion chambers to the energetic cosmic rays. Such studies are constrained by the techniques used for finding events in emulsion chambers which often involve scanning very many unwanted events. If emulsion chambers are combined with electronic detectors, as on the successful JACEE-3* flight**, events may be selected by charge and energy and located in the emulsion chamber using trajectory information also provided by electronic means.

A study was performed to evaluate the extension of the hybrid instrument approach for the continuation of these flight experiments into energy regions at which deconfinement of quarks from their nucleons has been predicted to occur in central nucleus-nucleus collisions.

---

*The Japanese-American Cooperative Emulsion Experiment-flight No. 3

**See JACEE contributions to the 19th International Cosmic Ray Conference, San Diego, 1985; Papers No.: HE1.4-1, HE1.4-2, HE1.4-3 OG4.1-9

DESIGN OF LARGE AREA HYBRID SYSTEM

Objectives

The primary objective of the experiment is to obtain 100 - 100 heavy nucleus interactions above 100 GeV/n for detailed analysis by emulsion techniques. The purpose of the electronic instrument, now well demonstrated by JACEE-3, is to permit the selection of the desired events without the work of tracing several thousand unwanted events. The electronic instrument must determine the charge and energy of each particle passing through the instrument and provide sufficiently accurate trajectory information so that events of particular interest can be located in the passive chambers. Though the shower (burst) counter provides a relatively poor energy measurement, its performance as a threshold or trigger energy detector has been demonstrated. Event statistics for the proposed instrument are for a typical 30 hr flight are shown for two trigger levels in table 1. Numbers were calculated from

$$N = I > (E_o) \cdot S\Omega T \cdot C_Z P_Z(E_o) \cdot P_{IZ}$$

where I is the primary integral spectrum, $S\Omega T$ is the exposure factor, C_Z the atmospheric transmission, P_Z the threshold function and P_{IZ} the interaction probability in the emulsion chamber.

An operational flight constraint of 5000 lbs including ballast (1800 lbs) was adopted, leaving the design goal of about 1200 lbs for the electronic detectors and mechanical support system (gondola). Since the pressurised vessel gondola must be dispensed with because of its weight, all electronics and detectors must be designed for operation at $\sim$5 Torr, at which pressure electrical and thermal problems must be addressed.

Table 1(a)

EXPECTED EVENT NUMBER IN EMULSION CHAMBER
AT ΣE_γ(threshold) = 1 TeV

	>Eo (GeV/n) >200	>500	>1000	>2000	Total No. of Triggered Events
$Z \geq 17$	40	10	3.1	0.9	62
	(56)	(14)	(4.3)	(1.3)	(87)
Ne-S	61	31	9.8	3.3	61
	(99)	(50)	(16)	(5.3)	(99)
C-O	74	60	25	8.6	74
	(138)	(111)	(47)	(16)	(138)
H_e	72	72	63	34	72
	(304)	(304)	(264)	(145)	(304)
P	230	230	230	230	230
	(1100)	(1100)	(1100)	(1100)	(1100)
TOTAL					
$Z \geq 6$	175	101	38	13	197
all	477	403	331	277	500

xx: number interacting in chamber

(xx): number at top of chamber

*Exposure Factor: $S\Omega T = 2.6 \times 10^5$ m^2 sr S

Table 1(b)

EXPECTED EVENT NUMBER IN EMULSION CHAMBER
AT ΣE_γ(threshold) = 3 TeV

Charge	>Eo (GeV/n) >200	>500	>1000	>2000	Total No. of Triggered Events
$Z \geq 17$	9.3	7.1	2.9	0.9	9.3
	(13)	(10)	(4)	(1.3)	(13)
Ne-S	9.2	9.2	7.4	2.9	9.2
	(15)	(15)	(12)	(4.8)	(15)
C-O	11	11	9.7	7.0	11
	(21)	(21)	(18)	(13)	(21)
H_e	9.7	9.7	9.7	9.7	9.7
	(41)	(41)	(41)	(41)	(41)
P	31	31	31	31	31
	(150)	(150)	(150)	(150)	(150)
TOTAL					
$Z \geq 6$	30	27	20	11	30
all	70	68	61	52	70

xx: number interacting in chamber

(xx): number at top of chamber

The new instrument is shown in figure 1 . It contains, apart from the emulsion chambers, the following elements which are discussed below in detail:

A. Charge Detector

A. Proportional Counter Hodoscope (PCH) for tracking

C. Support Structure

A. Charge Detector

(i) Design Goals

Techniques for charge detection are now standard practice in this laboratory and elsewhere and no developments were needed. A new approach was required to the engineering of the box itself, since the area of the radiator is approximately 9 times that of JACEE-3.

The charge resolution design goal is $\sigma(z) \leq 1$. This is derived by setting it equal to the known resolution of the other charge detector (CR-39) when the track-registration temperature is not known within a few degrees.

(ii) Selection of Radiator

Both scintillators and Cerenkov radiators were considered as light-emitters. Factors affecting the charge resolution obtainable with such materials includes: intrinsic photon production and fluctuations thereof, light collection efficiency, area non-uniformities, temperature dependency of PMT's and contamination of signal by back-flow of particles from an interaction in the emulsion chamber. The last effect was observed in JACEE-3 as an energy dependence of the charge detector signal above 20 GeV/n for Fe particles. Because most of the back-scattered particles are known to be of low-energy, Cerenkov radiator with threshold $\beta > 0.3$ was

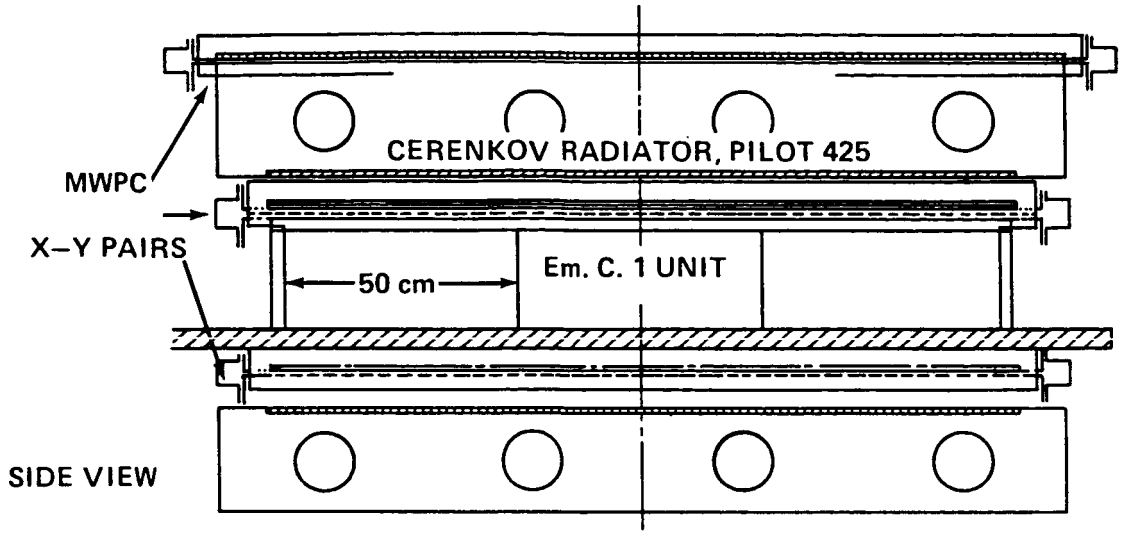

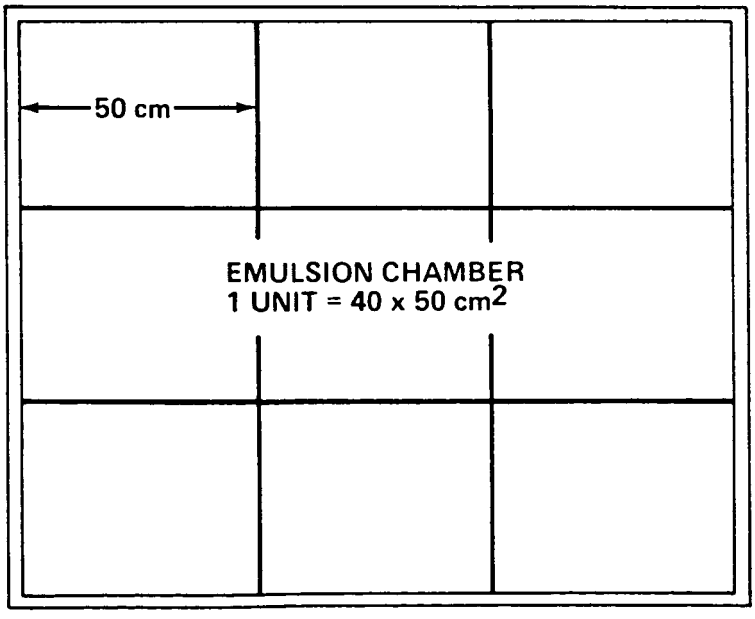

FIGURE 1. LARGE AREA HYBRID DETECTOR FOR EASY SELECTION OF HIGH ENERGY HEAVY COSMIC RAY INTERACTIONS FOR EMULSION CHAMBER ANALYSIS.

selected for this application since it is expected to be less sensitive to these particles than a scintillator.

(iii) Light Collection Efficiency and Charge Resolution

For a light diffusion box of total internal area A_t painted with white coating of reflectance r, and equipped with photomultipliers (PMT's) of total face-area A_p we may calculate the efficiency of collection of photons by the PMT's. Assumptions are that light emission (by Cerenkov or scintillation effect) is isotropic, that reflection from paint is diffuse and that no light is reflected from PMT faces.

Then, if $S = A_p/A_t$, the efficiency ε of collection is given by

$$\varepsilon = s/1-r(1-s)$$

The function ε is plotted versus r and s in figures 2+3 and for practical values of r and s. The calculated values agree well with actual tests and calibrations made in the laboratory.

From figures 2 and 3 it may be seen that at reflectances <.95 small changes in reflectance are unimportant, while above r = 0.97 the efficiency improves markedly with small changes in r. As a practical matter even the best $BaSO_4$ paint if not properly applied may have a reflectance of .95, while if proper procedures are used 0.98 is attainable. The practical range of s is limited by cost and weight. For a detector of this size s would be in the range of 0 to a few percent. For s = 2.5% we see that the collection efficiency ranges from 40 to 55% for paint reflectances in the range 0.96 to 0.98. It should be noted that the presence of a solid radiator may reduce the effective value of r from that of the reflectance coating. Measurements on a test diffusion box with s = 0.7% and measured

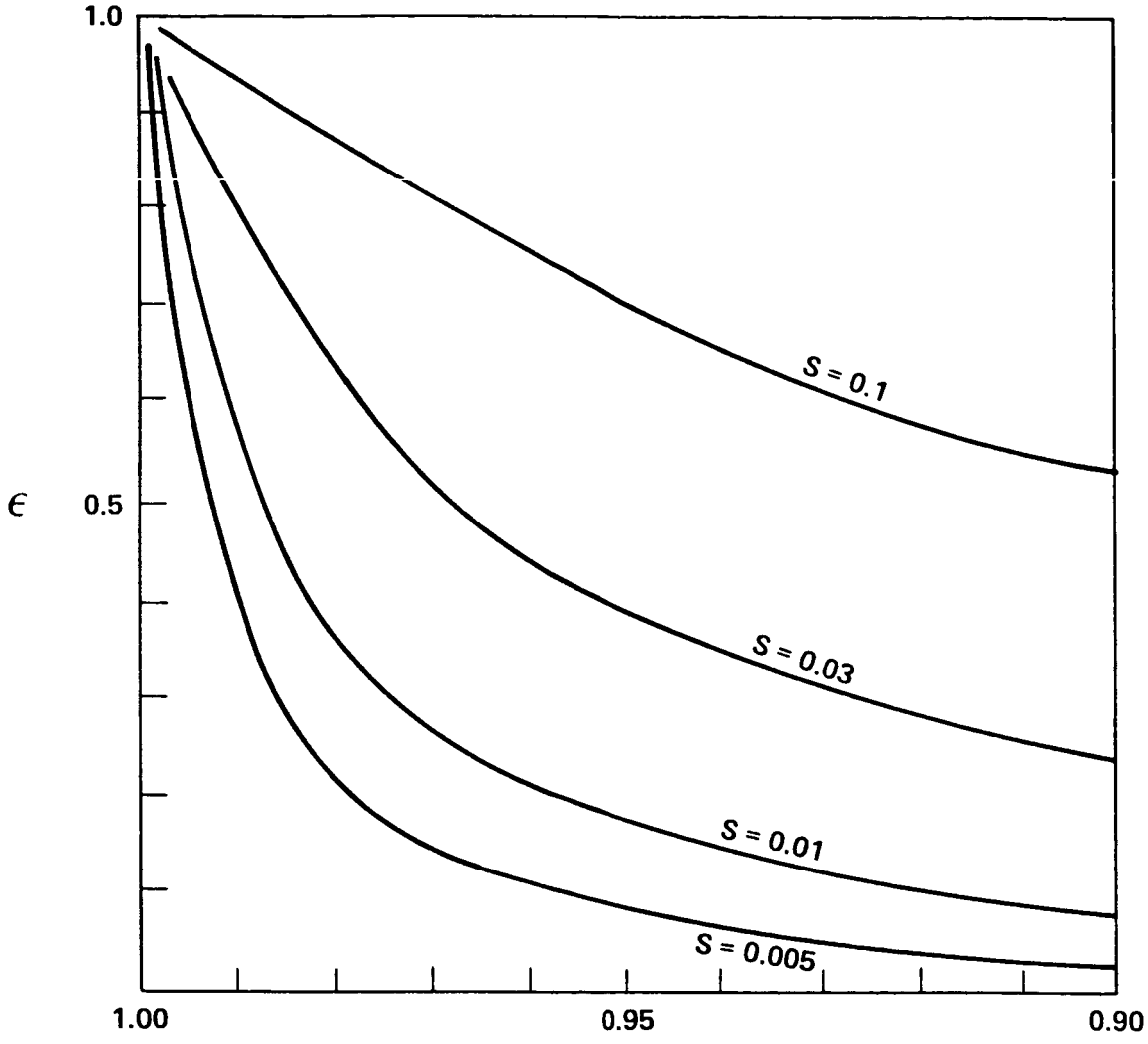

FIGURE 2. LIGHT-COLLECTION EFFICIENCY, ϵ, VS. PAINT REFLECTANCE FOR LIGHT-DIFFUSION BOXES. VALUES GIVEN FOR S-RATIOS OF 0.5% TO 10% (S = PMT FACE AREA/TOTAL INTERNAL AREA)

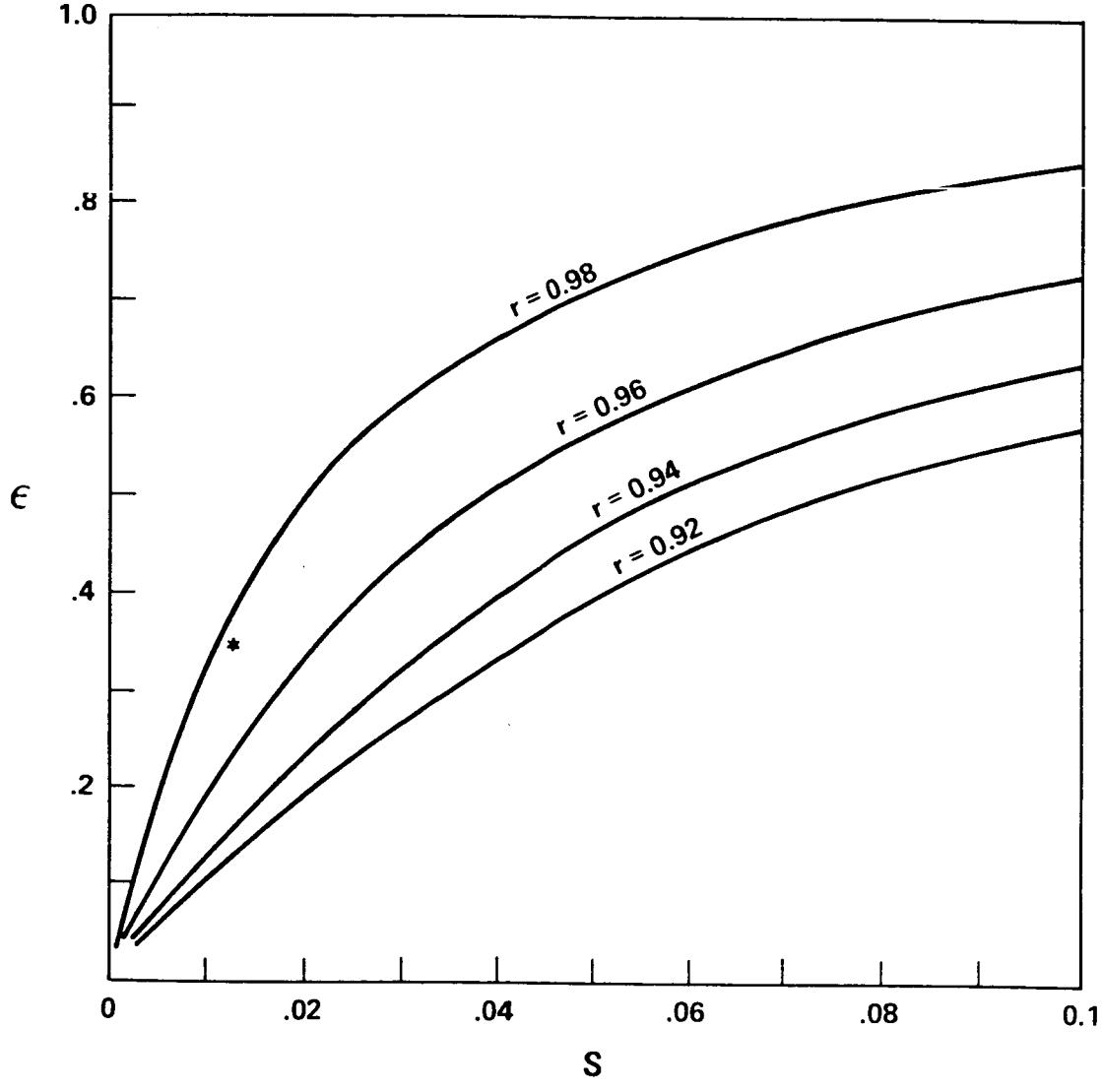

FIGURE 3. LIGHT-COLLECTION EFFICIENCY, ϵ, VS. S-RATIO (S = PMT AREA/TOTAL INTERNAL AREA). CURVES ARE FOR REFLECTANCES OF 0.92 TO 1.0. ASTERISK IS DATA FROM A FLIGHT GAS-CERENKOV COATED WITH GOOD QUALITY $BaSO_4$.

efficiency ε of $\sim$ 10% indicate (from figure 2.) that the effective reflectance in this case was 0.94.

From results of a previous flight Cerenkov counter (CP-76) we obtain the comparison:

Counter	Radiator	r(eff.)	s%	ε	n(pe)	σ_{pe} (charge units)
CP-76	½" Pilot 425	0.94	3.7	0.38	21	0.11
design	¼" Pilot 425	0.94	2.6	0.29	7.3	0.19

Other sources of random signal variation exist however, affecting the resolution:

$$\sigma^2 = \sigma^2_{pe} + \sigma^2_{\lambda} + \sigma^2_{sn} + \ldots$$

where σ_{λ} is the path-length uncertainty and σ_{sn} that due to system noise. An estimate of variances other than photoelectron statistics based on actual flight experience yields an effective charge resolution for the new detector design of $\sigma(z) \sim 0.3$ charge units. This resolution is adequate for the purpose.

Mechanical Design of Light-Diffusion Boxes for Charge and Burst Detectors

The boxes must accommodate plastic radiators 150 cm square lying on the bottom of the box and viewed by 12 PMT's mounted in the side walls. The PMT's with flange hardware were 19 cm in diameter. The nominal dimensions of the box were therefore set at 170 cm x 170 cm x 25 cm.

Design requirements of the box are: sufficient rigidity to support 37 lbs of radiator and 32 lbs of PMT hardware without distortion and rupture, absolute light-tightness, and low weight. The design approach used lightweight foam sandwich technology developed for aerospace use. The core selected was 0.75 polystyrene foam, clad with 0.006 in aluminum skins, bonded with a urethane-modified epoxy adhesive (Narmco 7343). The box was fabricated by a modular process, with the 4 sides, the bottom, and the top laid up and bonded separately. The foam core in each element was completely encapsulated, being provided with U-shaped edge members bonded in place on the panel assembly.

Bonding: Adhesive thickness was effectively controlled by transfer rolling in much the same fashion as is employed in inking a printing press, applying adhesive to both surfaces to be mated. Wooden support rings (for detector tube support) were inserted in cut-outs in the foam core, and bonded in the single component assembly process. Other inserts to provide attachment points for the plastic radiators and feed throughs for LED calibrators were placed at this time. Pressure was applied by covering the coated and assembled components with a 3-mil nylon film bag, pumping down,

and holding at 20-25 in Hg for 2 days. This process, and subsequent assembly operations, were carried out on a 7' x 7' plywood platen, specially constructed and levelled for the purpose, and sealed to prevent air leaks into the evacuated bag volume.

Assembly: The sides were bonded to the bottom plate with the same adhesive used in sandwich assembly; this bond was reinforced by bonding internal and external angle strips, internally and externally, at each panel juncture. These strips carry the principal load across the joint and add to longitudinal strength to better carry support and landing loads.
The completed box shown in figure 4 had good good rigidity and structural strength. Vacuum chamber tests showed that the design was adequate for balloon-flight deployment. PMT and plastic radiator mounting hardware has been fabricated for one unit. Weights of the completed article are

box, unpainted	32 lbs
PMT's, 16 x 2 lbs	32 lbs
plastic radiator	37 lbs
paint, insulation	9 lbs
TOTAL	110 lbs

(Note that the burst detector will need only 4 PMT's.)

The photomultiplier selected for use is the 5" EMI D302B. While this tube is fairly temperature sensitive, other attributes of conversion efficiency, ruggedness and low cost recommend it. Temperature sensors will be mounted to the face of the PMT's to monitor temperature variations during flight to allow corrections to the pulse-height data. Fittings for the light-emitting diode (LED) calibrators were fabricated. One will be mounted in the center of the detector for tube balancing and the other in

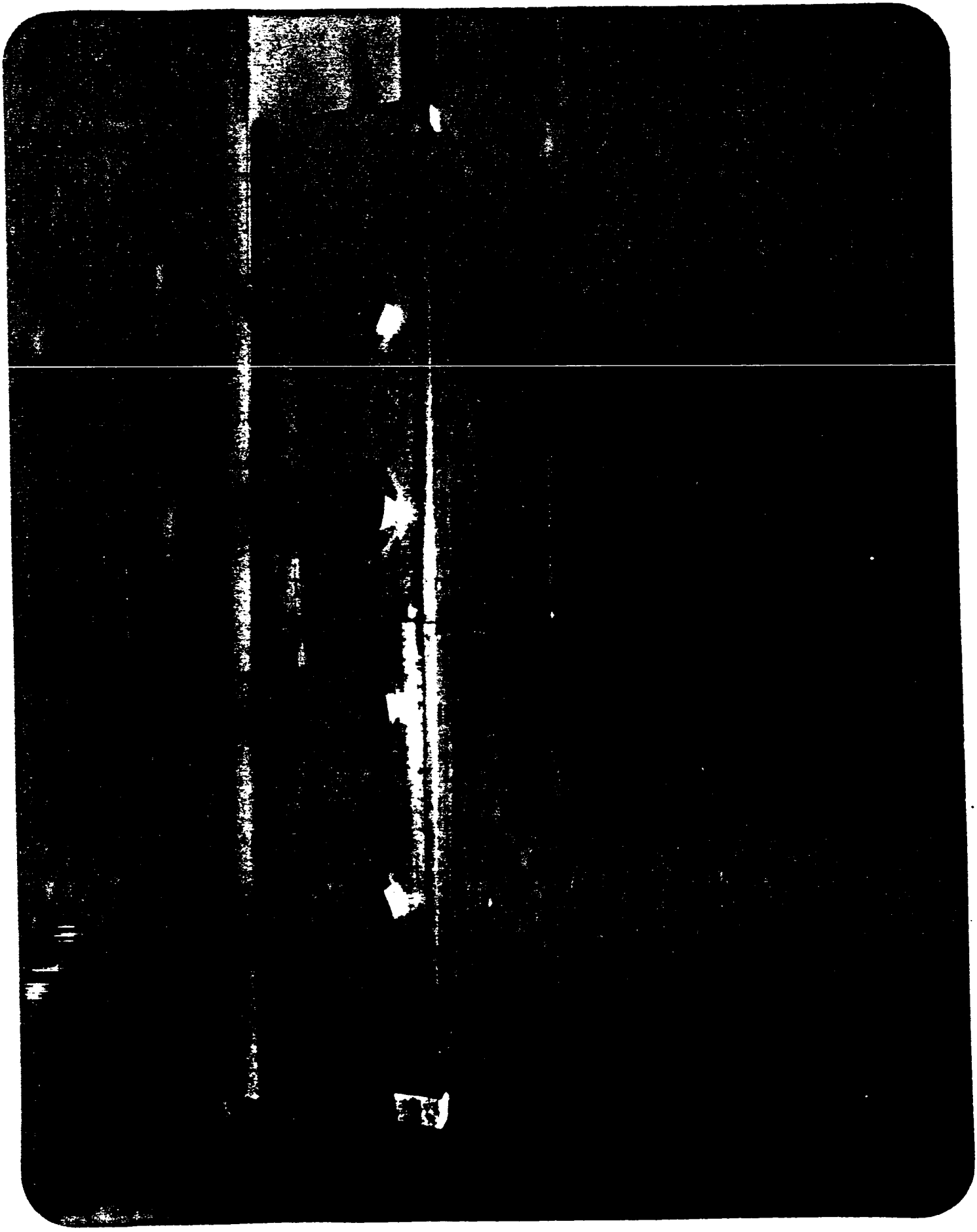

FIG. 4

one corner for anisotropy and dynamic range checking. Each LED is mounted in a 2 in. long aluminum tube so that the LED light is directed down into the radiator in a narrow cone and may not be directly viewed by any PMT.

B. Proportional Counter Hodoscope Design

Proportional counters possess many advantages for use in large area hodoscopes. These include adjustable gain and wide dynamic range of triggering particles, reliability, and relatively low cost. As discussed above, the multiwire counter technology developed at MSFC and successfully used on several balloon flights including JACEE-3 is not suited for application without a heavy enclosing pressure vessel. We have consequently adopted the basic approach of a JACEE group at the Institute for Cosmic Ray Research (ICR), the University of Tokyo, and introduced some improvements to make it suitable for large area hodoscopes. This approach, conceptually shown in figure 5, operates on the same physical principles as that used in JACEE-3 except that the counter gas is now retained by individual thin-walled aluminum tubes in close-packed arrays. An anode wire runs down the center of each tube, from which signals are amplified and processed.

The earliest version of the ICR cellular hodoscope was a 1 m x 1 m model using a soldering method for tube attachment and sealing to the end boxes. Following discussions with ICR personnel two major modifications were adopted. The first was the use of an epoxy construction technique to fuse all tubes together and seal the headers that contain the gas and electronics. The second was the introduction of spring tension on each anode to uniformly tension the anode, so that anode sag under gravity and varying tension due to thermal and structural forces was controlled. A 1.8

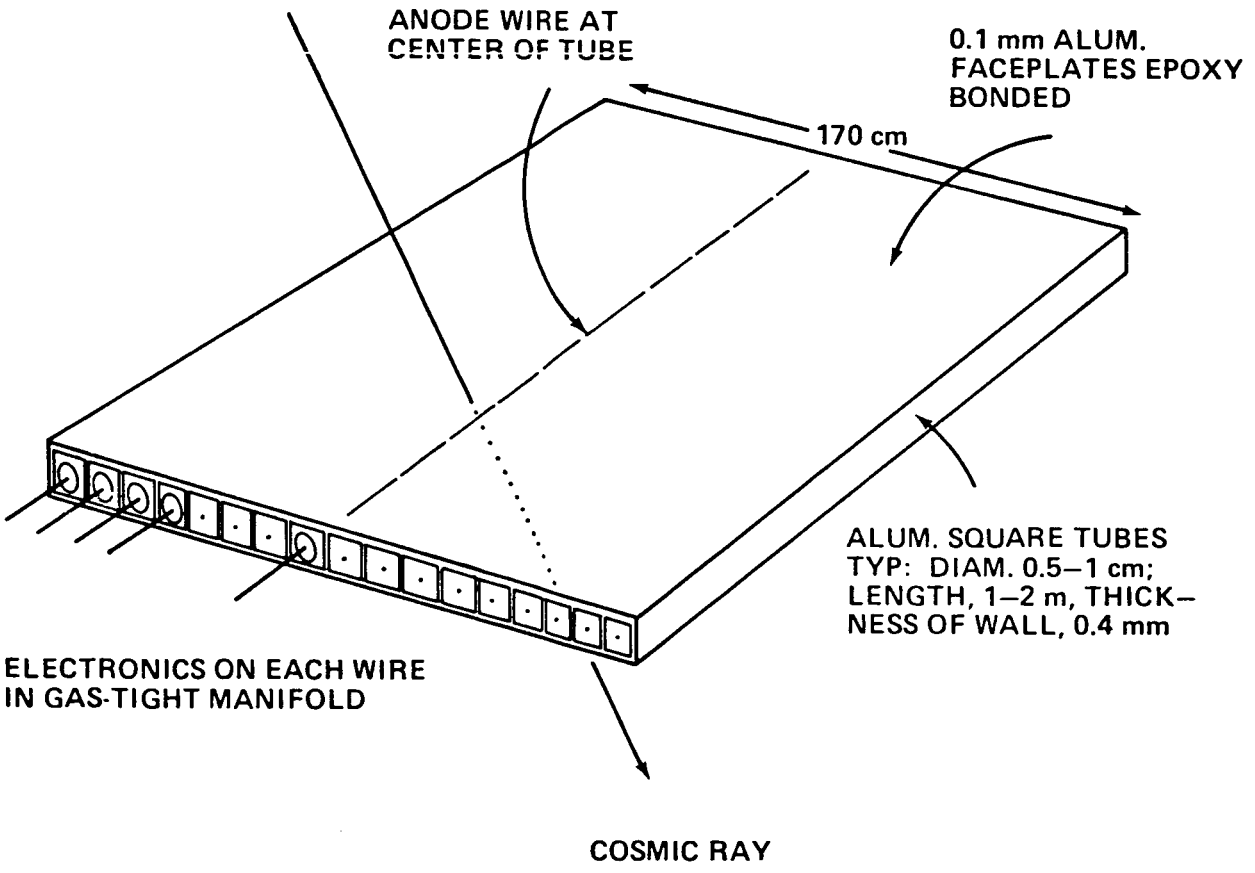

FIGURE 5. CONCEPTS OF CELLULAR PROPORTIONAL COUNTER HODOSCOPE

m x 1.8 m version of this hodoscope with these modifications(see figure 6) has been fabricated by the CI company of Tokyo, Japan and ICR personnel. It was successfully tested on a balloon flight in Japan in June 1985.

The readout of the hodoscope is performed by using high sensitivity discriminators on each anode wire which transfer any received anode signal during a one microsecond grating time to an attached shift register. The shift register has the same number of bits as the number of anodes in the plane, (180 in this case). Following the triggered event the register is shifted through 180 cycles by an external clock and the data is delivered at the clock count corresponding to the anode number. The discriminators and shift register are contained in the headers of each hodoscope layer as shown in figure 6. This allows a minimum number of electrical feed throughs into the gas volume, which is self contained in each plane. Feed throughs are required only for high voltage ($\sim$1800 volt), low voltage, clock in, and readout.

Of major importance in the design is the position and angular resolution of the hodoscope. Poorer resolution results in a larger area which must be searched in the CR39 plates and a larger number of background tracks which may be confused with the track of interest. An analysis of this problem is given below in terms of cell size and other instrument parameters.

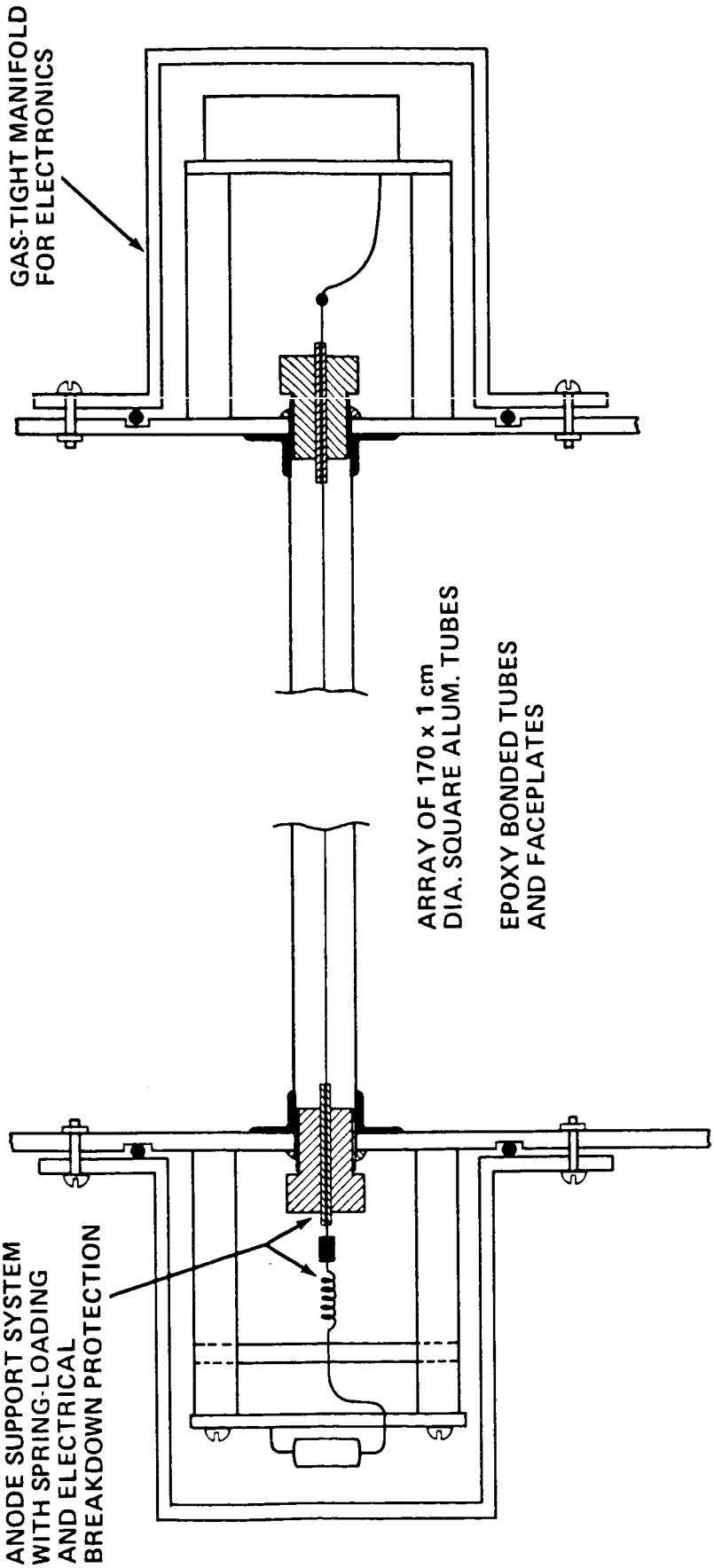

FIGURE 6. DESIGN SKETCH OF CELLULAR PCH

(ii) Tracking Error Analysis

The parameters affecting confusion in locating particles chosen by electronic criteria depend on the size of the error region in Δx, Δy, $\Delta\theta$, $\Delta\phi$, Δz and the number of background tracks of similar character within this error box. The background number, for the cosmic rays, depends chiefly on the flight exposure time and the geomagnetic latitude of the flight. Hodoscope parameters may be expressed as shown:

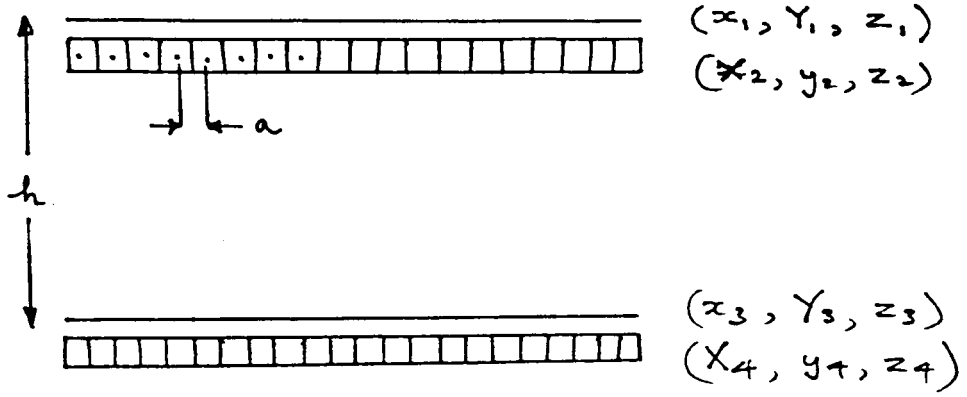

For a given track, zenith angle θ, and azimuthal angle ϕ, Y_1 and X_4 are calculated by:

$$\tan\theta = \frac{\sqrt{(x_1 - x_3)^2 + (y_2 - y_4)^2}}{z_3 - z_1} = \frac{\sqrt{(x_1 - x_3)^2 + (y_2 - y_4)^2}}{h}$$

$$\tan\phi = \frac{y_2 - y_4}{x_1 - x_3}$$

$$Y_1 = y_2 + (z_1 - z_2)\tan\theta\sin\phi - y + a\tan\theta\sin\phi$$

$$X_4 = x_3 + (z_3 - z_4)\tan\theta\cos\phi = x_3 + a\tan\theta\cos\phi$$

Practically the uncertainty in x, y $\sim$ a (the cell size).

Then $$\sigma(X,Y) = a\sqrt{1 + 2\left(\frac{z_1 - z_2}{z_3 - z_1}\right)^2}$$

$$= a\sqrt{1 + 2(a/h)^2}$$

$$\sigma(X,Y) \sim a \text{ for } a << h$$

(a = 1 cm, h = 30 cm in this case)

$$\sigma(\tan\theta) = \frac{\sqrt{2}.a}{h} \quad \text{(constant)}$$

$$\sigma(\phi) = \frac{\sqrt{2}.a}{h \tan\theta} \text{ radian}$$

The search region is then defined by:

$$\text{Area} = 2a \times 2a = 4a^2$$

$$\text{Solid Angle} = 4\,\delta\phi\,\frac{m\,\delta m}{(1 + m^2)^2} \quad (\text{where } m \equiv \tan\theta)$$

$$= \frac{8\,a^2}{h^2(1 + m^2)^2} = 8.9 \times 10^{-3} \times \frac{1}{(1 + m^2)^2}$$

$$\Delta\Omega \text{ (max)} = 8.9 \times 10^{-3} \text{ steradian (for } m = 0)$$

The requirement for no confusion is that there shall be a density less than 1 particle/$\Delta A.\Delta\Omega$ to avoid mis-tracking.

Maximum acceptable background of similar tracks

$$= \frac{\pi}{8.9 \times 10^{-3} \times 4} \text{ cm}^{-2}$$

$$= \underline{88 \text{ tracks cm}^{-2}}$$

for the geometry considered here.

Calculated background levels are shown in Table II for two geomagnetic cutoff conditions corresponding to Palestine, Texas, (R_c = 4.3 GV) and Hawaii, (R_c = 13.3 GV).

Table II

CALCULATED BACKGROUND TRACK DENSITY (30 HOUR FLIGHT)

	R_c = 4.3 GV (Tracks/cm^2)	R_c = 13.3 GV (Tracks/cm^2)
$Z \geq 17$	13	2.7
Ne-S	36	6.8
C-O	130	27

It is concluded from this analysis that tracks could be correlated between the PCH and the emulsion chamber for elements Ne-Fe without ambiguity for a typical flight from Palestine, Texas. If the flight were at the out-off rigidity of Hawaii, track location would be much easier at all z's and would be feasible down to CNO.

While it is clear that smaller tube sizes give better resolution and easier tracking, there are practical difficulties to be considered, some of which are:

- increased complexity and weight of electronics which scales with anode wire number.

- difficulties with anode wire sag and array-plane distortion are worse with smaller tube sizes.

A practical limitation for tube-size is in the 5 to 10 mm diameter range for arrays up to 2 m long. This is determined not so much by anode wire sag which is < 1 mm in the center at the proper tension, but by bending of the array under various forces deriving from accumulated anode tension, attachment stresses, differential thermal expansion, and gravity. A tube diameter of 1 cm has been chosen for the design of the flight system.

FLIGHT GONDOLA AND STRUCTURAL SUPPORT SYSTEM

Structural Design Specification

The project consisted of the design and analysis of the structural aspects of the main platform and cables supporting the instrumentation.

The gondola had to meet the following specifications:

- o ability to support a 1800 pound evenly distributed load
- o ability to support 2300 pounds of ballast
- o means for cable attachment
- o means of keeping the cables free from entanglement
- o cradle system should be included to support gondola and payload before launch

Other design criteria included:

- o cost should be minimized
- o total weight of parts that fly should be minimized
- o use of commercially available parts and materials
- o use of minimum number of parts for ease of assembly
- o reduce the bulk of spreader for ease of transport

Design Description

The instrumentation is supported on a platform suspended from the balloon by cables at the corners. The platform consists of an aluminum honeycomb sandwiched between two aluminum skins. The honeycomb arrangement was chosen for its high structural rigidity and low weight. The skins distribute the loads more evenly and provide a flat surface for attachment of the emulsion chambers.

The honeycomb is bounded by four C-channels mitered at the corners and adhered to the honeycomb. Cables run from the corners of the C-channels to

the balloon. The cables pass through holes in the channels and are swaged to prevent them from pulling through.

The cable spreader prevents the cables from making contact with the instrumentation and prevents them from becoming entangled. The spreader consists of an aluminum framework lying in the plane perpendicular to the cables. The design maintains a fixed distance between the cables, preventing them from tangling. In addition, it maintains a fixed clearance between the cables and the instruments. The frame design also minimizes the cost and weight of the structure.

The spreader is held in place by aluminum tubing that runs from the platform to the spreader. This tubing is secured by the cables and diagonal wires, forming a stable truss-like structure. The cables pass through the tubing up to the spreader and then angle to a point above the spreader where they converge and attach to the parachute fixture.

Legs are adjoined underneath the corners of the platform to prevent the lower instrumentation from crushing under the weight of the structure.

All components used in the design were sized to meet the performance requirements without wasting materials. In addition, readily available parts were used wherever possible to avoid costly manufacturing expenses.

The only parts which would require special machining are the corner pieces of the cable spreader. These are constructed from aluminum tubing mitered to form a ninety degree angle. An eyelet is welded to the outside corner; a triangular plate is welded to the inside corner. The main cables pass through the eyelet and the diagonal support wires fasten to a hole drilled in the plate. The compression members of the spreader slide into the corner pieces, which may have to be bored for ample clearance.

Perfomance

Complete stress analyses were performed for the components of the structure. Calculations for the more critical elements may be found in the Appendix. Additional calculations can be found in the design notebooks.

The calculations were performed using conservative, but reasonable factors of safety. A static factor of safety of two was used throughout. An additional dynamic factor of safety of three was imposed on load-bearing members during flight to accomodate parachute-opening shock loads.

Table 1 shows the critical parameters involved in the analysis of various members. The factors of safety given represent the margin of safety above the previously mentioned factors used in the stress calculations. This added margin of safety results from the use of stock sizes.

Load-bearing members were analyzed according to their worst case. For the vertical columns supporting the spreader, this was considered to be ground handling forces. Those members bearing significant loads in flight were analyzed for reactions to parachute shock.

Conclusions

A drawing of the gondola and support system design is shown in figure 7. As this structure is flight hardware, the safety and structural soundness of the system were considered paramount. After observing the results of the first flight, it may be possible to reduce factors of safety. At this point, however, the effects of ground handling, parachute shock and adverse flight conditions are, to some degree, speculative. The approach used in this design maximizes the possibility of a successful flight.

The design provides rigid supports under the spreader allowing reasonably facile ground calibration and tune up with the cables and spreader attached. If the latter could be left detached until just before launch, the rigid supports could be omitted, reducing weight and cost and facilitating handling.

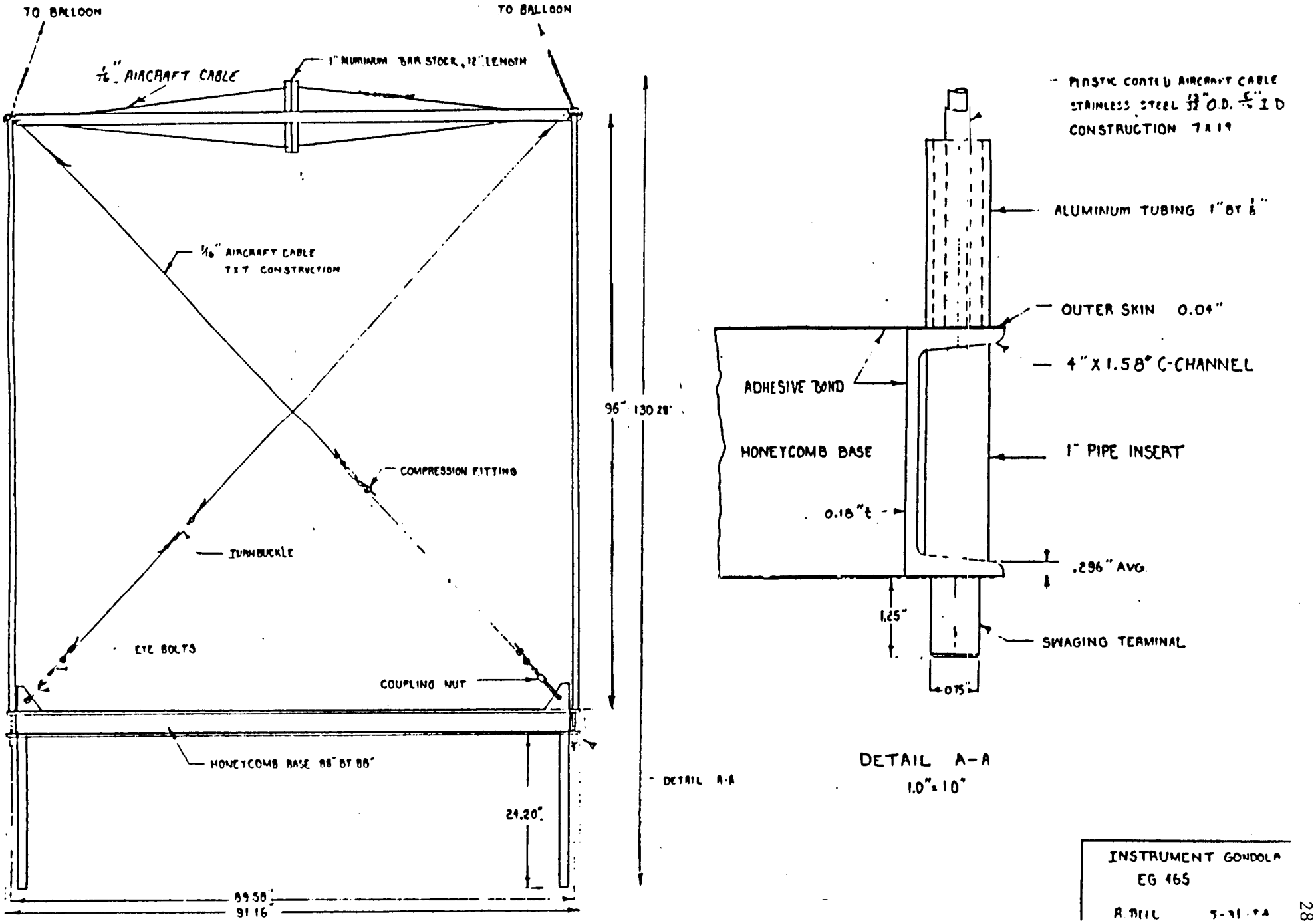

Figure . Support-System Design for Hybrid Instrument

E. INSTRUMENT SUMMARY

EMULSION CHAMBERS

9 Chambers, 40 x 50 x 25 cm^3	
Weight, including boxes	1062 kg

CHARGE COUNTER

Diffusion Box 170 x 170 x 25 cm^3	
16 D302B PMT's, Analyzed in 4 Banks	
Radiator 150 x 150 x .635 cm Pilot 425	
Weight	50 kg

Burst Counter

Diffusion Box 170 x 170 x 25cm^3	
4 D302B PMT's, Individually analyzed	
Radiator 150 x 150 x .635 cm Plastic Scintillator	
Weight	41 kg

Hodoscopes

Cellular PCH, 3 x Y pairs	
1 cm square tubes filled with P10 gas	
resolution 1 cm^2 and 2^o	
Weight	150 kg

Support Structure

Honeycomb Platform, Struts	
Weight	115 kg

Electronics, Batteries

(Preamps, amps, discriminators, ADC's Triggering System, Calibration, Housekeeping, Digital Data, High Voltage)	
Weight	78 kg

TOTAL WEIGHT, SCIENTIFIC INSTRUMENT	1486 kg (3270 lbs)